Deep-learning-based automated measurement of outer retinal layer thickness for use in the assessment of age-related macular degeneration, applicable to both swept-source and spectral-domain OCT imaging

JIE LU,[1] **YUXUAN CHENG,**[1] **FARHAN E. HIYA,**[2] **MENGXI SHEN,**[2] **GISSEL HERRERA,**[2] **QINQIN ZHANG,**[3] **GIOVANNI GREGORI,**[2] **PHILIP J. ROSENFELD,**[2] **AND RUIKANG K. WANG**[1,4,*]

[1]*Department of Bioengineering, University of Washington, Seattle, Washington, USA*
[2]*Department of Ophthalmology, Bascom Palmer Eye Institute, University of Miami Miller School of Medicine, Miami, Florida, USA*
[3]*Research and Development, Carl Zeiss Meditec, Inc., Dublin, CA, USA*
[4]*Department of Ophthalmology, University of Washington, Seattle, Washington, USA*
*wangrk@uw.edu

Abstract: Effective biomarkers are required for assessing the progression of age-related macular degeneration (AMD), a prevalent and progressive eye disease. This paper presents a deep learning-based automated algorithm, applicable to both swept-source OCT (SS-OCT) and spectral-domain OCT (SD-OCT) scans, for measuring outer retinal layer (ORL) thickness as a surrogate biomarker for outer retinal degeneration, e.g., photoreceptor disruption, to assess AMD progression. The algorithm was developed based on a modified TransUNet model with clinically annotated retinal features manifested in the progression of AMD. The algorithm demonstrates a high accuracy with an intersection of union (IoU) of 0.9698 in the testing dataset for segmenting ORL using both SS-OCT and SD-OCT datasets. The robustness and applicability of the algorithm are indicated by strong correlation (r = 0.9551, P < 0.0001 in the central-fovea 3 mm-circle, and r = 0.9442, P < 0.0001 in the 5 mm-circle) and agreement (the mean bias = 0.5440 um in the 3-mm circle, and 1.392 um in the 5-mm circle) of the ORL thickness measurements between SS-OCT and SD-OCT scans. Comparative analysis reveals significant differences (P < 0.0001) in ORL thickness among 80 normal eyes, 30 intermediate AMD eyes with reticular pseudodrusen, 49 intermediate AMD eyes with drusen, and 40 late AMD eyes with geographic atrophy, highlighting its potential as an independent biomarker for predicting AMD progression. The findings provide valuable insights into the ORL alterations associated with different stages of AMD and emphasize the potential of ORL thickness as a sensitive indicator of AMD severity and progression.

1. Introduction

Age-related macular degeneration (AMD) is a leading cause of permanent vision loss among individuals aged 50 and above [1,2]. Vision loss is typically associated with the late-stage AMD, which manifests as geographic atrophy (GA) and/or exudative AMD [2]. While the U.S. Food and Drug Administration (FDA) has approved first treatment, intravitreal pegcetacoplan, for slowing the rate of GA growth [3], there is currently no effective treatment available to stop the formation or progression of GA [4]. Therefore, there remains an urgent need to identify early, clinically measurable features that can serve as biomarkers to help predict the eyes at highest risk

for progression to GA for use in clinical trials designed to intervene earlier and prevent disease progression.

Optical coherence tomography (OCT) has revolutionized the field of ophthalmology by providing high-resolution three-dimensional (3D) images of retinal layers [5–8]. These images offer invaluable insights into the microstructural and microvascular changes that arise and progress in eyes with AMD. The progression of these changes over time plays a crucial role in the staging, treatment planning, and monitoring of AMD. The widespread use of OCT in ophthalmology has facilitated the identification of OCT biomarkers associated with the progression from early to late AMD. These biomarkers include the central drusen volume [9–12], the presence of calcified/refractile drusen [13–15], hyperreflective foci [16–18], reticular pseudodrusen [18–20], choriocapillaris flow deficits [21], and outer retinal atrophy (including photoreceptor degeneration) [22–24]. Among these risk factors, assessing photoreceptor degeneration in OCT imaging presents a significant challenge, both technically and clinically.

Using a deep learning strategy, Orlando et al. [25] assessed the photoreceptor degeneration by measuring the distance between the top of the ellipsoid zone (EZ) and the outer boundary of the interdigitation zone, where photoreceptor loss was considered to occur when an axial distance measurement was equal to or less than 4 μm. The study demonstrated the successful utilization of photoreceptor loss and thinning as valuable indicators for evaluating the efficacy of GA treatment [26,27]. However, despite significant advances in OCT development in research labs [28,29], quantifying EZ loss and thickness using commercially available OCT devices is still challenging due to the influences of various shadow artifacts (e.g., shadows from vessels and various overlaying lesions), the limited axial resolution of OCT devices used, the extremely thin nature of the EZ [25–27,30,31], and the OCT directional effect when imaging the outer retina especially over drusen [32,33]. As an alternative strategy, outer retinal layer (ORL) thickness may serve as a surrogate marker for assessing photoreceptor degeneration. This is because the imaging features of photoreceptor degeneration, such as external limiting membrane (ELM) descent, ELM and EZ disruption, and the subsidence of inner nuclear layer (INL) and outer plexiform layer (OPL) [20], contribute to the thinning of the ORL. Zhang et al. [34] reported a significant negative correlation between ORL thickness around GA and the annual enlargement rate of GA, suggesting ORL thickness can be used a potential marker for assessing photoreceptor degeneration.

Several automated algorithms have been developed and tested to automatically segment retinal layers on OCT images, including the methods using active contour [35], graph search [36–37], and deep learning approaches [38–44], which may be leveraged to measure the ORL thickness. However, each method has its own limitations. For example, traditional computer vision methods face challenges in handling pathologic changes, such as the discontinuity of the OPL likely caused by the GA formation, making it difficult to achieve an optimal balance between disease-related disruptions and spatial connectivity. Studies that employ deep/machine learning methods for retinal layer segmentation on OCT imaging have primarily focused on spectral domain OCT (SD-OCT) datasets [38,39,41–43,45–48], leaving a clear need for developing an algorithm for ORL segmentation that can be applied to both SD-OCT and SS-OCT scans.

In medical image segmentation, convolutional neural networks (CNNs) have emerged as the dominant approach due to their ability to learn highly complex features and models across different levels of feature abstraction from training data [49]. Among the various architectures available, U-Net [50], which consists of a symmetric encoder-decoder network, stands out as the most widely adopted. However, CNN-based models heavily rely on the convolution operation, which poses challenges in accounting for long-range relation due to its intrinsic local nature. The vision transformer (ViT), designed for sequence-to-sequence prediction with global self-attention mechanisms, is considered a viable alternative to CNNs [51], but can result in limited localization abilities due to insufficient low-level details. In 2021, TransUNet was proposed as a novel model

that successfully integrated detailed, high-resolution spatial information from CNNs with the global context encoded by ViT [52]. While the TransUnet model has demonstrated promise in retinal layer segmentation of SD-OCT images of normal and diabetic macular edema eyes [42,43], it remains unclear whether it is applicable to SS-OCT datasets, and whether it can be used to help segment the clinical features involved in AMD such as accurately segmenting the ORL.

In this study, we propose an automated algorithm employing TransUNet architecture, capable of measuring the ORL thickness from the scans acquired by both SS-OCT and SD-OCT imaging. To demonstrate the effectiveness of the algorithm, we performed a comparative analysis of ORL thickness measurements from SS-OCT and SD-OCT imaging. To further investigate whether the ORL thickness could serve as a useful biomarker for predicting the progression of AMD, we examined variations in ORL thickness among different stages of AMD, including normal eyes, eyes with intermediate AMD displaying macular reticular pseudodrusen, eyes with intermediate AMD displaying soft drusen only, and eyes with late nonexudative AMD characterized by the presence of persistent choroidal hypertransmission defects (hyperTDs) on OCT scans [11].

2. Methods

This prospective OCT imaging study was approved by the Institutional Review Board of the University of Miami Miller School of Medicine. The study was performed in accordance with the tenets of the Declaration of Helsinki and complied with the Health Insurance Portability and Accountability Act of 1996. Through a retrospective review of subjects enrolled from April 2016 to August 2022, a total of 199 eyes were included, comprising 80 normal eyes without any ocular disease, 30 eyes with intermediate AMD with macular reticular pseudodrusen, 49 eyes with intermediate AMD displaying typical soft drusen only, and 40 eyes with eyes with late nonexudative AMD characterized by the presence of persistent choroidal hyperTDs.

2.1. Image acquisition

Two optical coherence tomography (OCT) instruments were utilized in this study: the PLEX Elite 9000 (Carl Zeiss, Meditec Inc., Dublin, CA) for SS-OCT imaging and the Cirrus 5000 HD-OCT (Carl Zeiss, Meditec Inc., Dublin, CA) for SD-OCT imaging. This SD-OCT instrument utilized a central wavelength of 840 nm and a scan rate of 68,000 A-scans/second. The scanning pattern for the 6 × 6 mm SD-OCT scan consisted of 350 A-scans per B-scan and 350 B-scans per volume, with each B-scan repeated twice using the macular cube protocol. This scanning pattern resulted in a uniform spacing of 17 μm between A-scans. The SS-OCT instrument used a central wavelength of 1050 nm and a scan rate of 100,000 A-scans/second. The 6 × 6 mm SS-OCT scan pattern included 500 A-scans per B-scan and 500 B-scans per volume, with each B-scan repeated twice using the macular cube protocol. This scanning pattern provided a uniform spacing of 12 μm between A-scans. Both instruments featured a full width at half maximum axial resolution of ~5 μm in tissue and an estimated transverse resolution of ~15 μm at the retinal surface.

A total of 40 eyes presenting with typical soft drusen and 40 eyes with hyperTDs, underwent both SS-OCT and SD-OCT scanning. The remaining 119 eyes (80 normal eyes, 30 reticular pseudodrusen eyes and 9 drusen eyes) underwent SS-OCT scanning only.

2.2. Automated segmentation of the outer retinal layer

In this study, the ORL is defined as the region extending from the inner boundary of the outer plexiform layer (OPL) to the retinal pigment epithelium (RPE) when the RPE is visible [34]. In cases where there is complete RPE and outer retina atrophy (cRORA, or hyperTDs), the ORL is defined as the region extending from the OPL to Bruch's membrane (BM).

Figure 1 shows the architecture of the TransUNet model used in this study, with the specifications all labeled. The modified TransUNet model includes an encoder, decoder, and bottleneck. Unlike

the original TransUNet that had three layers [42,43], the encoder block is composed of four convolutional layers and employs ReLU activation. This modification aims to extract more profound features from OCT images, such as texture information encountered in the AMD eyes. Following this, a bottleneck block is introduced, featuring six transformer layers instead of the original twelve in the original TransUNet model. This implementation applies multi-head self-attention to image patches, facilitating the capture of long-range contextual relationships within the extracted features from preceding encoder block. The primary goal of this modification is twofold: 1) to mitigate overfitting and 2) to improve computation efficiency. Finally, a decoder block with four transpose convolutional layers is utilized to up-sample the feature maps, restoring their shape to match the original input data.
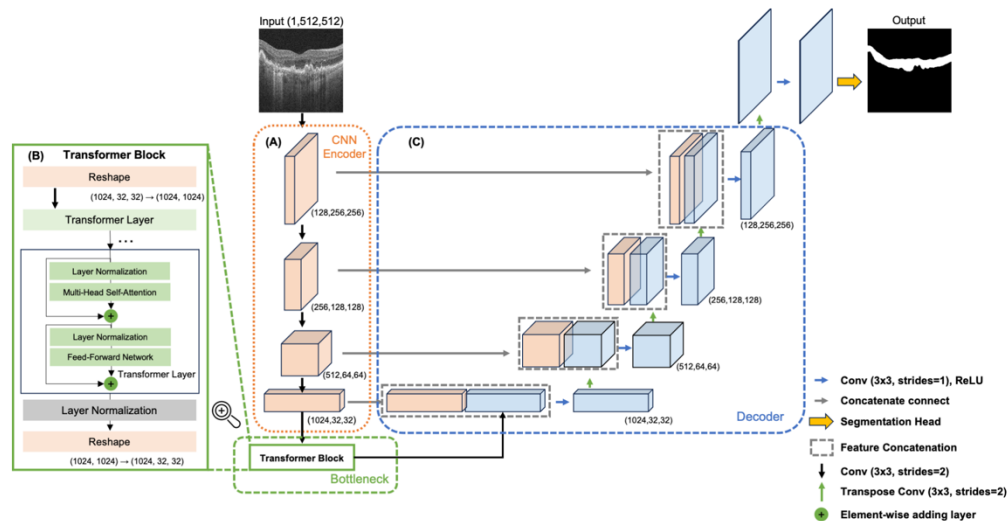

Fig. 1. The modified TransUNet model architecture and specifications used to perform outer retinal layer segmentation. (A) the schematic of the encoder block composed of four convolutional layers; (B) the schematic of the bottleneck block composed of six transformer layers; (C) the schematic of the decoder block composed of four transpose convolutional layers.

The Adam optimizer with a learning rate of 0.0001 was used, the model evaluation metric was defined as the intersection over union (IoU), and the loss function utilized for training was the binary crossentropy loss. This model was trained with 200 epochs with a patience for early stopping of 30 epochs, and only the model with the best metric was saved when the validation loss was not updated under 30 training epochs. For this study, the model was implemented in Keras using TensorFlow 2.9.0 as the backend, and training was conducted using a 24GB NVIDIA 4090 GPU.

With the confirmed information of clinical diagnoses, the boundaries that define the ORL were annotated from a total of 2,000 representative OCT B-scans by two clinical experts (F.H. and G.H.) using a custom-built software that was improved from the segmentation and annotation software package originally developed in [53]. The purpose of the manual segmentation was for training the model. The consensus on the annotation of ORL boundaries was reached between both graders. In cases of disagreement, a senior grader (P.J.R.) was the adjudicator. For training purposes, we utilized 32 labeled eyes, with 16 eyes (i.e., 800 B-scans) from SS-OCT and 16 eyes (i.e., 800 B-scans) from SD-OCT. Within the training dataset, we further applied a 75:25 split between training and validation at the eye level to ensure an effective and reliable evaluation process. The remaining 8 labeled eyes, comprising 4 eyes (i.e., 200 B-scans) from SS-OCT and

4 eyes (i.e., 200 B-scans) from SD-OCT, were reserved for testing. These B-scans were extracted from 20 volumes of SS-OCT scans and 20 volumes of SD-OCT scans, respectively. These scans were obtained from a total of 40 eyes out of the 199 eyes included in the study. The composition of the 20 SS-OCT volume scans encompassed 2 normal eyes, 2 eyes with macular reticular pseudodrusen (RPD), 8 eyes with drusen, and 8 eyes with hyperTDs. The 20 SD-OCT volume scans comprised 10 eyes with drusen and 10 eyes with hyperTDs. Importantly, there was no overlap between the eyes included in the SS-OCT and SD-OCT scans within the training dataset. To consider the practical and pathological manifestations of AMD features in the OCT scans, the selected B-scans encompassed a diverse range of imaging features including normal scans, a range of soft drusen sizes, calcified drusen, hyperreflective foci, macular reticular pseudodrusen, and hyperTDs. The details of the training and testing datasets are shown in Table 1. To avoid over down-sampling of input images in the A-line direction, all images were first automatically cropped to 512 (A-line direction) $\times$ 500(SS-OCT)/350(SD-OCT) pixels and then were resized to 512×512 pixels.

Table 1. Training and testing datasets[a]

	Training	Validation	Testing
Number of eyes (SS-OCT/ SD-OCT)	24 (12/12)	8 (4/4)	8 (4/4)
Number of representative B-scans (SS-OCT/ SD-OCT)	1200 (600/600)	400 (200/200)	400 (200/200)

[a]Datasets were obtained from normal eyes and eyes with reticular pseudodrusen, intermediate and large drusen, calcified drusen, hypertransmission defects, and hyperreflective foci

2.3. Measurements of drusen volume and area of hyperTDs

The measurements of drusen volume were automatically obtained from an algorithm using the optical attenuation coefficient (OAC) enhanced RPE elevation relative to BM (namely OAC elevation), which was cross-validated by the Advanced RPE Analysis Algorithm version 0.10, a validated algorithm publicly available on the Advanced Retinal Imaging Network website (Carl Zeiss Meditec, Inc) [54]. The hyperTD areas were obtained with a semi-automatic algorithm that uses customized composite en face OAC images and customized en face sub-RPE OCT images from a slab defined by boundaries from 64 to 400 μm under BM. The details of the process have been described in our previous study [55]. Drusen volume and hyperTD areas were specifically measured in the 3-mm and 5-mm fovea-centered circles.

2.4. Statistical analysis

Statistical analysis was carried out using Matlab2021b and GraphPad Prism (GraphPad Software, San Diego, CA). Pearson's correlation was used to compare the ORL thickness measurements from SS-OCT and SD-OCT, and Bland Altman plots were used to analyze the agreement between the ORL thickness measurements from SS-OCT and SD-OCT. One-way analysis of variance (ANOVA) and Tukey–Kramer post-hoc tests were used to compare ORL thickness differences between normal, reticular pseudodrusen, drusen and hyperTD groups. Furthermore, the relationship between ORL thickness and drusen volume in the drusen group and the relationship between ORL thickness and hyperTD areas in the hyperTD group were studied by Pearson's correlation. P values below 0.05 were considered statistically significant.

3. Results

The original U-Net and the modified Trans U-Net models were trained separately using the same datasets as shown in Table 1. Table 2 shows their specific IoUs for the training, validation, and

testing datasets. In the eight eyes or 400 B-scans in the testing set, the modified Trans U-Net model significantly outperformed the original U-Net model (IoU: 0.9698 vs 0.9198).

Table 2. Training and testing results

Intersection Over Union (IoU)	Original U-Net	Modified TransUNet
Training	0.9574	0.9850
Validation	0.9522	0.9748
Testing	0.9189	0.9698

Figure 2 demonstrates the automatic ORL segmentation of two representative eyes with drusen and hyperTD, respectively, that were scanned by both SD-OCT and SS-OCT instruments at the same visit. Note that these eyes were not included in the training and validating datasets. Overall, the automated segmentations and measurements show excellent agreement between the results from the SS-OCT and those from the SD-OCT scans.
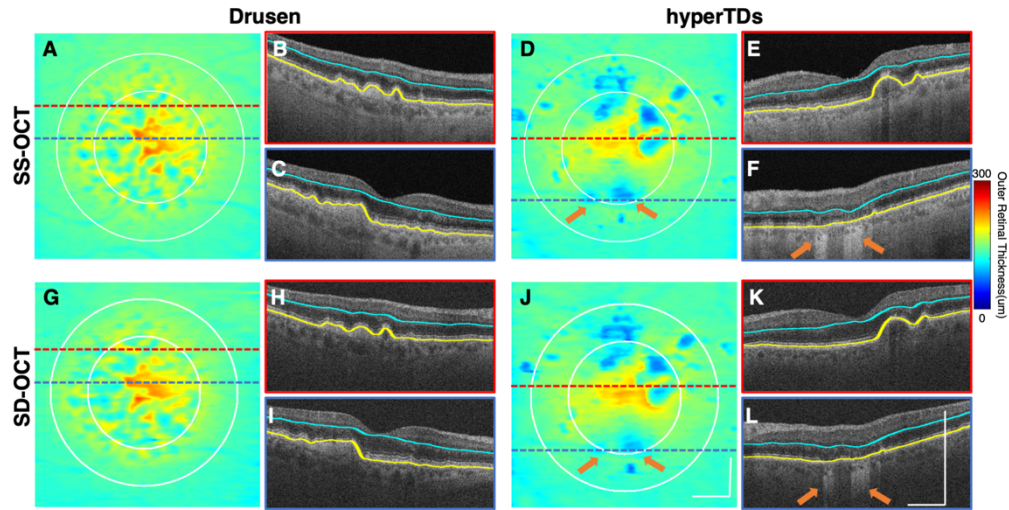
Fig. 2. Representative automatic segmentation results of outer retinal layer (ORL) taken from an eye with soft drusen and an eye with persistent hypertransmission defects (hyperTDs) scanned by both SS-OCT (top row) and SD-OCT (bottom row). (A, D, G, and J) ORL thickness maps encoded using the color bar. (B, C, E, F, H, I, K and L) OCT B-scans with their locations shown as dashed lines in (A, D, G, and J) where drusen and hyperTDs can be identified. Orange arrows indicate the hyperTDs that are used clinically to identify atrophic areas. Blue outlines indicate the inner boundary of the outer plexiform layer and yellow outlines indicate the retinal pigment epithelium (RPE) or Bruch's membrane where RPE is absent. White circles indicate 3 mm and 5 mm diameter fovea-centered circles. Scale bar represents 1 mm.

In total, 40 eyes with only typical soft drusen and 40 eyes with hyperTDs underwent both SS-OCT and SD-OCT scanning and the ORL thickness measurements were compared from both imaging platforms. Among the 80 eyes used for evaluation, 32 eyes were utilized during the algorithm's training. It is worth noting that there was no overlap between the eyes included in the SS-OCT and SD-OCT scans within our training dataset. This indicates that for each eye, at least one volume scan (either SS-OCT or SD-OCT) used for evaluation was not part of the algorithm's training data. Therefore, the reuse of the data from the 32 eyes is unlikely to significantly influence the algorithm's evaluation. Figure 3 shows the scatter plots for the

automated measurements of ORL thickness acquired by the SS-OCT vs the SD-OCT instruments. A strong correlation was found between the measurements of ORL thickness in the 3-mm circle (r = 0.9551, P < 0.0001, Fig. 3 A) and 5-mm (r = 0.9442, P < 0.0001, Fig. 3 B) fovea-centered circles. Bland-Altman analysis showed that the average bias of the measurements in the 3-mm circle was 0.5440 um (95% limits of agreement [−8.005, 9.093], Fig. 3 C) and the average bias of the corresponding measurements in the 5-mm circle was 1.392 um (95% limits of agreement [−5.335, 8.119], Fig. 3 D) between SS-OCT and SD-OCT scans. Overall, the measurements of ORL thickness computed using the SS-OCT appear to be a little thicker than those produced by the SD-OCT, particularly in hyperTD eyes and when the mean ORL thickness was less than 150 μm. However, considering the axial pixel dimension of 2 μm, this discrepancy between SD and SS-OCT would not be considered clinically significant.
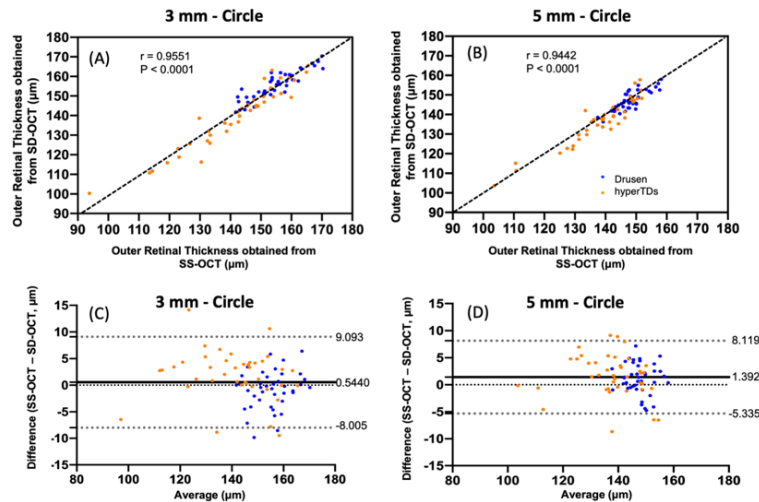

Fig. 3. Automated measurements of outer retinal layer (ORL) thickness from OCT scans acquired by the SS-OCT vs the SD-OCT. (A) Scatter plot of the ORL measurements from SS-OCT against SD-OCT showing strong correlation in the 3 mm (r = 0.9551, P < 0.0001), and (B) in 5 mm (r = 0.9442, P < 0.0001) fovea-centered circles. (C and D) Bland-Altman agreement analysis of ORL measurements from SS-OCT against SD-OCT, where the solid line represents the bias, and the dashed gray lines represent the upper and lower 95% limits of agreement. Blue dots represent drusen eyes, and orange dots represent eyes with persistent choroidal hypertransmission defects.

After validation of the algorithm above, we investigated its utility in the measurements of changes in the ORL thickness in the eyes with intermediate and late stages of AMD. In this exercise, a total of independent 199 eyes scanned by SS-OCT were measured and analyzed. Among these 199 eyes, there were 80 normal eyes, 30 macular reticular pseudodrusen eyes, 49 drusen only eyes, and 40 hyperTD eyes. The characteristics of these groups are summarized in Table 3. The four groups were age matched (ANOVA P = 0.1087), with the mean age being 72.5 ± 8.0 years in the normal group, 73.6 ± 8.2 years in the macular reticular pseudodrusen group, 76.0 ± 8.0 years in the soft drusen group, and 74.1 ± 8.7 in the hyperTD group. Figure 4 shows representative examples of each group. Note that these four examples were not used in the training dataset. Compared with the normal eye, the ORL thickness map of the macular reticular pseudodrusen eye is globally thinner (Figs. 4(B) and (F)), while the ORL thickness map for the drusen eye (Figs. 4(C) and (G)) shows thinning overlying the drusen. The ORL thickness map of the hyperTD eye is significantly thinner than other three groups due to the attenuation and loss of the photoreceptors and RPE in the regions of atrophy (Figs. 4 D and H).
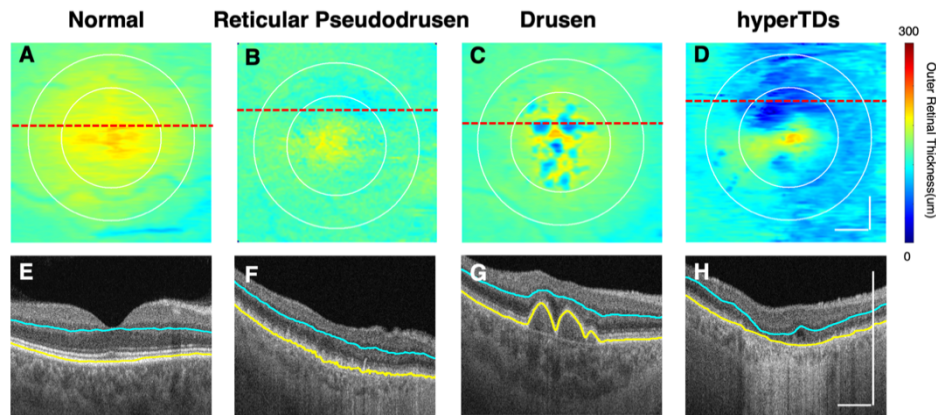
Fig. 4. Representative segmentation results of the outer retinal layer (ORL) taken from a normal eye (A and E), a reticular pseudodrusen eye (B and F), a soft drusen eye (C and G), and an eye with a persistent choroidal hypertransmission defect (D and H). (A-D) ORL thickness maps where the ORL thickness is encoded according to the color bar. (E-H) OCT B-scans with their locations shown as dashed lines in (A-D), with blue lines indicating the inner boundary of outer plexiform layer (OPL) and yellow lines indicating the location of retinal pigment epithelium (RPE) or Bruch's membrane where RPE is absent. Blue lines and yellow lines were derived from the automated segmentations. White circles indicate 3 mm and 5 mm diameter fovea-centered circles, respectively. Scale bar represents 1 mm.

Table 3. Characteristics of all the eyes imaged with SS-OCT included in this study[a]

Characteristics	Normal (n = 80)	RPD (n = 30)	Drusen (n = 49)	hyperTDs (n = 40)	P Value
Age, year, mean (SD)	72.5(8.0)	73.6(8.2)	76.0(8.0)	74.1(8.7)	0.1087
3mm-circle ORL thickness, µm, mean (SD)	178.1(9.4)	167.7(8.6)	156.3(8.9)	141.3(16.3)	<0.0001
5mm-circle ORL thickness, µm, mean (SD)	163.1(8.7)	156.0(7.4)	148.7(5.5)	138.3(11.3)	<0.0001

[a]**Abbreviations**: SD – standard deviation. ORL – outer retinal layer. RPD – reticular pseudodrusen. hyperTDs – hypertransmission defects.

Table 3 and Fig. 5 and Table 3 show the results for the ORL thickness measurements representing all eyes in the 3-mm circle and 5-mm fovea-centered circles. When comparing the average ORL thickness of each group with the average of every other group, it was observed that the normal group presented the largest mean value, followed by the macular reticular pseudodrusen group, the soft drusen group with the third largest mean value, and finally, the hyperTD group with the lowest mean value. These findings highlight significant differences of ORL thickness between the groups (all P < 0.01) in both the 3-mm circle and 5-mm fovea-centered circles. The absolute differences between means may change with different datasets due to variations in soft drusen volume and areas of hyperTDs, but the relationships between the groups are expected to remain the same.

Figure 6 shows the relationship between the measurements of ORL thicknesses and drusen volume in the soft drusen group. Notably, a significant negative correlation between drusen volume and ORL thickness was observed within the 3 mm-circle (r = -0.4616, P = 0.0008), whereas no significant correlation was found within the 5 mm-circle (r = -0.1175, P = 0.4215). In other words, in the 3 mm circle a smaller ORL thickness appeared to correspond to a larger
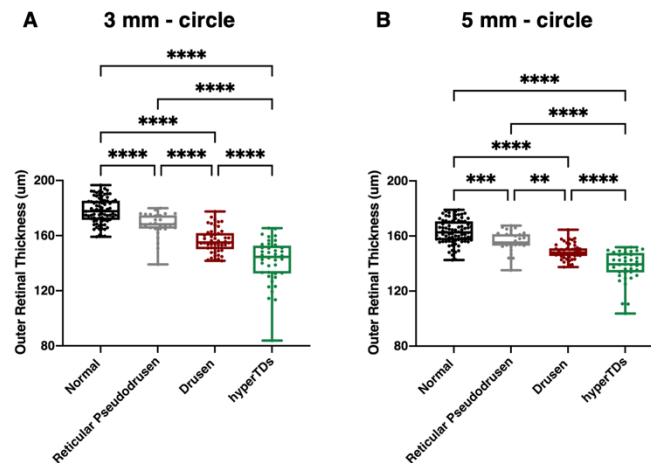
Fig. 5. Graphic representation of automated outer retinal layer (ORL) thickness measurements using the algorithm developed in this study. Comparison of ORL thickness among the normal, reticular pseudodrusen, soft drusen, and persistent choroidal hypertransmission defects on the 3 mm (A) and 5 mm (B) fovea-centered circles, respectively. ** represents $P \leq 0.01$, *** represents $P \leq 0.001$, and **** represents $P \leq 0.0001$. Boxplots show interquartile range, whiskers minimum to maximum, and all points.

RPE-BM distance. The difference in results between the circles might be due to the fact that most of the drusen were typically located within the 3 mm circle, as seen in Fig. 6(A).
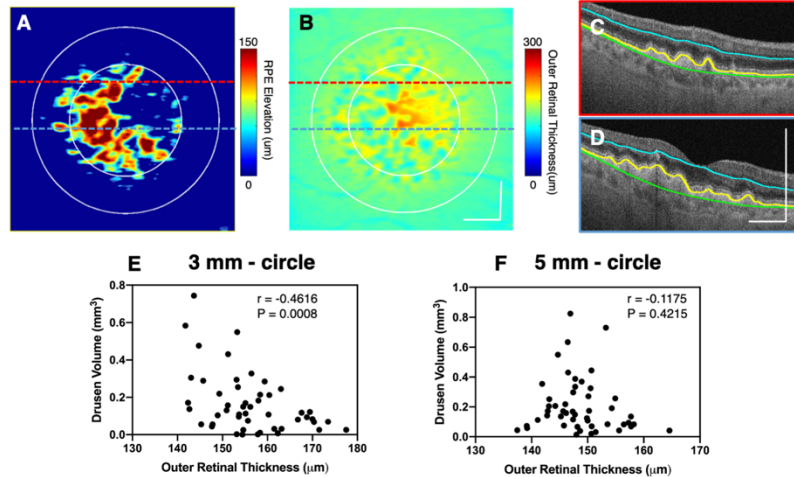

Fig. 6. A representative example of a drusen eye along with the relationship between drusen volume and ORL thickness measurements in the drusen group: (A) the drusen map by displaying the distances between yellow lines and green lines shown in (C and D) and (B) corresponding outer retinal layer (ORL) thickness map. (C and D) OCT B-scans with their locations shown as dashed lines in (A and B) where drusen can be identified. Blue outlines indicate the inner boundary of the outer plexiform layer, yellow outlines indicate the retinal pigment epithelium (RPE), and green outlines indicate Bruch's membrane. (E and F) Scatter plots showing the relationship between drusen volume and ORL thickness measurements in the drusen group for the 3 mm-circle and 5 mm-circle centered on the fovea, respectively. White circles indicate 3 mm and 5 mm diameter circles centered on the fovea.

Figure 7 shows the relationship between the ORL thickness measurements and the hyperTD area measurements in the GA group. The hyperTD regions had a thinner ORL thickness than surrounding regions, so a strong negative correlation between hyperTD areas and ORL thickness observed within both the 3 mm-circle (r = -0.8333, P < 0.0001) and the 5 mm-circle (r = -0.7630, P < 0.0001) would be expected.
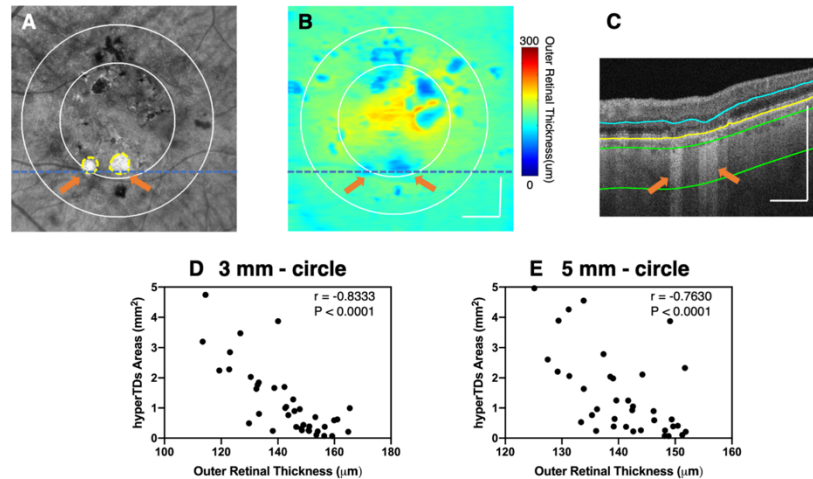

Fig. 7. A representative example of an eye with persistent choroidal hypertransmission defects (hyperTDs) along with relationship between hyperTD area measurements and ORL thickness measurements in the persistent hyperTD group: (A) OCT En face Sub-RPE image obtained from a slab defined from 64 um to 400 um below the Bruch's membrane (BM) shown with green lines in (C), with the yellow outlines highlighting the GA areas and (B) corresponding outer retinal layer (ORL) thickness map. (C) OCT B-scan with its location shown as the dashed line in (A and B) where hyperTDs can be identified. Orange arrows indicate the hyperTDs that are used clinically to identify atrophic areas. Blue outlines indicate the inner boundary of the outer plexiform layer and yellow outlines indicate the retinal pigment epithelium (RPE) or Bruch's membrane where RPE is absent. (D and E) Scatter plots showing the relationship between hyperTD area measurements and ORL thickness measurements in the persistent hyperTD group in the 3 mm-circle and 5 mm-circle centered on the fovea, respectively. White circles indicate 3 mm and 5 mm diameter fovea-centered circles.

4.   Discussion

There remains an urgent need to identify OCT biomarkers that can be used to define clinical endpoints that can predict the high risk of progression to late AMD. Photoreceptor degeneration has been associated with AMD progression [22–24,34]. To investigate whether ORL thickness could serve as a surrogate biomarker for assessing photoreceptor degeneration and predicting the risk of AMD progression, we have developed a deep learning-based automated algorithm capable of measuring the thickness of the ORL that is applicable to both SS-OCT and SD-OCT scans. The deep learning-based approach demonstrated a high accuracy in segmenting the ORL, with an IoU of 0.9698 in the testing dataset, allowing for reliable quantification of disease-related changes caused by the loss of RPE, elevation of RPE, subsidence of OPL, and disruption of the photoreceptor integrity. Strong correlation and agreement of ORL thickness measurements between SS-OCT and SD-OCT datasets further validated the robustness and applicability of the algorithm across different OCT modalities (Fig. 2 and 3). In addition to its application in evaluating AMD, ORL thickness has also been utilized for the detection of brain-related diseases

[56,57] and diabetic macular edema [58], highlighting the potential future applications of the algorithm.

Using this automated algorithm, we showed significant differences in ORL thickness among the normal, macular reticular pseudodrusen (intermediate AMD), soft drusen (intermediate AMD), and hyperTD (late AMD) groups (Table 3 and Figs. 4 and 5), consistent with previous studies demonstrating that intermediate AMD had thinner ORL compared to normal controls [59–61]. The extent of this thinning is likely correlated with the volume of the drusen. It is worth noting that Sotaro et al. [62] reported no age-related changes in ORL thickness, while Arepalli et al. [63] found an increase in ORL thickness with age in the normal group. Using the current ORL algorithm, we plan to explore whether the ORL thickness changes with age. While it is likely that the reduced ORL thickness observed in our study depends more on the anatomic changes associated with soft drusen and hyperTDs rather than an effect of age alone, it is intriguing to speculate that the decreased macular thickness associated with macular reticular pseudodrusen is not due to the anatomic presence of reticular pseudodrusen since the RPE and not the EZ serves as the outer boundary of the ORL algorithm. Therefore, the outer retinal thinning in eyes with reticular pseudodrusen is likely real and probably secondary to the poor nutritional exchange that results from decreased choriocapillaris perfusion as previously reported for these eyes [19].

Drusen volume, known to be a predictor of disease progression of late AMD [9,64], showed a negative correlation with ORL thickness in the 3-mm fovea-centered circle (r = -0.4616, P = 0.0008, Fig. 6). However, there was no significant correlation between drusen volume and ORL thickness in the 5-mm circle. This is likely attributable to the influence of drusen volume on the measurements of ORL thickness, particularly considering that the majority of drusen were located in the fovea centered 3-mm circle in all the 49 drusen cases, as shown in the example in Fig. 6(A). An anticipated outcome would involve the ORL displaying a thinner dimension when situated above larger drusen. This is primarily due to the potential displacement and subsequent degeneration of photoreceptors directly overlying these drusen structures [65]. Consequently, a more pronounced inverse correlation emerges, correlating an escalation in drusen volume with a reduction in ORL thickness within the 3 mm circle. Notably, the interstitial space flanked by the 3 mm and 5 mm circles exhibits a diminished drusen presence, consequently leading to a dissipation of the correlation and statistical significance evident within the 3 mm circle, thus explaining its absence within the 5 mm circle. Also, this relationship between higher drusen volumes and ORL thinning may also explain the significant difference in ORL thickness between the drusen and reticular pseudodrusen groups shown in Fig. 5. In this study, the mean drusen volume within the fovea-centered 5 mm circle was 0.207 ± 0.185 mm^3 in the soft drusen group, whereas only 0.01 ± 0.02 mm^3 in the reticular pseudodrusen group were observed. Consequently, the ORL thickness in the drusen eyes were affected not only by drusen volume but also by outer retinal atrophy, while reticular pseudodrusen eyes were primarily impacted by outer retinal atrophy [60,61]. With these results, it is likely that the ORL thickness could serve as a more sensitive biomarker for evaluating the progression of AMD than drusen volume, as it encompasses changes from both drusen volume and the outer retina atrophy, which may correlate with decreased choriocapillaris perfusion. While encouraging, such statement warrants a systematic study by enrolling more eyes including different stages of AMD.

Strong correlations were observed between hyperTD area measurements and ORL thickness measurements in both the 3-mm and 5-mm circles (r = -0.8333, P < 0.0001 in the 3-mm circle; r = -0.7630, P < 0.0001 in the 5-mm circle; shown in Fig. 7). This correlation can be attributed to the significantly thinner ORL thickness in the hyperTD regions compared to the surrounding areas [66], shown in Fig. 4 (D and H). These findings highlight the potential of ORL thickness as a potential biomarker for assessing the progression of hyperTDs as previously reported [34].

Although promising, it should be noted that there are several limitations in the current study. First, the training datasets used in this study were obtained from Carl Zeiss OCT devices, and

the applicability of the algorithm to data acquired by other commercial devices, for example Heidelberg Engineering and Topcon, remains untested. Nevertheless, although some bias may arise when applying the algorithm to datasets from different device types, we believe our algorithm can still assist in annotating ORL segmentations in the scans acquired from these devices, and that our current algorithm can be trained to include them. Secondly, the lack of follow-up visits for the AMD groups hinders a comprehensive investigation of the impact of ORL thickness on AMD progression. To address this, future studies will incorporate multiple follow-up visits [67], enabling a comparison of ORL differences between eyes that progress to late AMD and those that do not, thus enhancing our knowledge of the mechanism and evolution of AMD. Lastly, this study did not measure other biomarkers associated with AMD, including choriocapillaris flow deficits, calcified drusen, and hyperreflective foci [68–70]. Together with the changes in ORL thickness measurements, we intend to investigate all these biomarkers in future studies to determine their predictive power in assessing AMD progression.

In conclusion, a deep learning-based algorithm was developed to measure ORL thickness as a surrogate marker for assessing AMD severity. The algorithm demonstrated high accuracy and robustness in quantifying ORL thickness measurements in different stages of AMD and is applicable to both SS-OCT and SD-OCT scans. The comparative analysis revealed significant differences in ORL thickness measurements among different AMD stages, indicating its potential use as an independent biomarker for predicting AMD progression as previously reported for the growth of hyperTDs [34].

References

1. W. L. Wong, X. Su, X. Li, *et al.*, "Global prevalence of age-related macular degeneration and disease burden projection for 2020 and 2040: a systematic review and meta-analysis," Lancet Glob Health **2**(2), e106 (2014).
2. M. Fleckenstein, T. D. L. Keenan, R. H. Guymer, *et al.*, "Age-related macular degeneration," Nat Rev Dis Primers **7**(1), 31 (2021).
3. J. S. Heier, E. M. Lad, F. G. Holz, *et al.*, "Pegcetacoplan for the treatment of geographic atrophy secondary to age-related macular degeneration (OAKS and DERBY): two multicentre, randomised, double-masked, sham-controlled, phase 3 trials," Lancet **402**(10411), 1434–1448 (2023).
4. K. Csaky, C. A. Curcio, R. F. Mullins, *et al.*, "New approaches to the treatment of age-related macular degeneration (AMD)," Exp. Eye Res. **221**, 109134 (2022).
5. T. T. Hormel and Y. Jia, "OCT angiography and its retinal biomarkers [Invited]," Biomed. Opt. Express **14**(9), 4542–4566 (2023).
6. P. J. Rosenfeld, G. Gregori, and R. K. Wang, "Unleashing the power of optical attenuation coefficients in OCT imaging of the retina," Biomed. Opt. Express **14**(9), 4947–4963 (2023).
7. C.-L. Chen and R. K. Wang, "Optical coherence tomography based angiography [Invited]," Biomed. Opt. Express **8**(2), 1056–1082 (2017).
8. E. A. Swanson and J. G. Fujimoto, "The ecosystem that powered the translation of OCT from fundamental research to clinical and commercial impact [Invited]," Biomed. Opt. Express **8**(3), 1638–1664 (2017).

9. N. S. Abdelfattah, H. Zhang, D. S. Boyer, *et al.*, "Drusen volume as a predictor of disease progression in patients with late age-related macular degeneration in the fellow eye," Invest. Ophthalmol. Visual Sci. **57**(4), 1839–1846 (2016).

10. Z. Chu, Y. Shi, X. Zhou, *et al.*, "Optical coherence tomography measurements of the retinal pigment epithelium to Brruch membrane thickness around geographic atrophy correlate with growth," Am. J. Ophthalmol. **236**, 249–260 (2022).

11. J. Liu, M. Shen, R. Laiginhas, *et al.*, "Onset and progression of persistent choroidal hypertransmission defects in intermediate age-related macular degeneration: a novel clinical trial endpoint," Am. J. Ophthalmol. **254**, 11–22 (2023).

12. A. Rivail, W.-D. Vogl, S. Riedl, *et al.*, "Deep survival modeling of longitudinal retinal OCT volumes for predicting the onset of atrophy in patients with intermediate AMD," Biomed. Opt. Express **14**(6), 2449–2464 (2023).

13. J. Liu, R. Laiginhas, M. Shen, *et al.*, "Multimodal imaging and en face OCT detection of calcified drusen in eyes with age-related macular degeneration," Ophthalmology Science **2**(2), 100162 (2022).

14. J. Lu, Y. Cheng, J. Li, *et al.*, "Automated segmentation and quantification of calcified drusen in 3D swept source OCT imaging," Biomed. Opt. Express **14**(3), 1292–1306 (2023).

15. A. C. S. Tan, M. G. Pilgrim, S. Fearn, *et al.*, "Calcified nodules in retinal drusen are associated with disease progression in age-related macular degeneration," Sci. Transl. Med. **10**(466), eaat4544 (2018).

16. K. Hirabayashi, H. J. Yu, Y. Wakatsuki, *et al.*, "OCT risk factors for development of atrophy in eyes with intermediate age-related macular degeneration," Ophthalmology Retina **7**(3), 253–260 (2023).

17. H. Zhou, J. Liu, R. Laiginhas, *et al.*, "Depth-resolved visualization and automated quantification of hyperreflective foci on OCT scans using optical attenuation coefficients," Biomed. Opt. Express **13**(8), 4175 (2022).

18. M. Nassisi, J. Lei, N. S. Abdelfattah, *et al.*, "OCT risk factors for development of late age-related macular degeneration in the fellow eyes of patients enrolled in the HARBOR study," Ophthalmology **126**(12), 1667–1674 (2019).

19. J. Li, Z. Liu, J. Lu, *et al.*, "Decreased macular choriocapillaris perfusion in eyes with macular reticular pseudodrusen imaged with swept-source OCT angiography," Invest. Ophthalmol. Visual Sci. **64**(4), 15 (2023).

20. M. Kong, S. Kim, and D.-I. Ham, "Incidence of late age-related macular degeneration in eyes with reticular pseudodrusen," Retina **39**(10), 1945–1952 (2019).

21. M. Thulliez, Q. Zhang, Y. Shi, *et al.*, "Correlations between choriocapillaris flow deficits around geographic atrophy and enlargement rates based on swept-source OCT imaging," Ophthalmology Retina **3**(6), 478–488 (2019).

22. G. J. Jaffe, U. Chakravarthy, K. B. Freund, *et al.*, "Imaging features associated with progression to geographic atrophy in age-related macular degeneration: classification of atrophy meeting report 5," Ophthalmology Retina **5**(9), 855–867 (2021).

23. M. Li, C. Huisingh, J. Messinger, *et al.*, "Histology of geographic atrophy secondary to age-related macular degeneration: a multilayer approach," RETINA **38**(10), 1937–1953 (2018).

24. R. Dolz-Marco, C. Balaratnasingam, J. D. Messinger, *et al.*, "The border of macular atrophy in age-related macular degeneration: a clinicopathologic correlation," Am. J. Ophthalmol. **193**, 166–177 (2018).

25. J. I. Orlando, B. S. Gerendas, S. Riedl, *et al.*, "Automated quantification of photoreceptor alteration in macular disease using optical coherence tomography and deep learning," Sci. Rep. **10**(1), 5619 (2020).

26. S. Riedl, W.-D. Vogl, J. Mai, *et al.*, "The effect of pegcetacoplan treatment on photoreceptor maintenance in geographic atrophy monitored by artificial intelligence–based OCT analysis," Oph Retina **6**(11), 1009–1018 (2022).

27. J. Mai, S. Riedl, G. S. Reiter, *et al.*, "Comparison of fundus autofluorescence versus optical coherence tomography–based evaluation of the therapeutic response to pegcetacoplan in geographic atrophy," Am. J. Ophthalmol. **244**, 175–182 (2022).

28. B. Lee, S. Chen, E. M. Moult, *et al.*, "High-speed, ultrahigh-resolution spectral-domain OCT with extended imaging range using reference arm length matching," Trans. Vis. Sci. Tech. **9**(7), 12 (2020).

29. T. Zhang, A. M. Kho, R. J. Zawadzki, *et al.*, "Visible light OCT improves imaging through a highly scattering retinal pigment epithelial wall," Opt. Lett. **45**(21), 5945–5948 (2020).

30. J. P. Ehlers, R. Zahid, P. K. Kaiser, *et al.*, "Longitudinal assessment of ellipsoid zone integrity, subretinal hyperreflective material, and subretinal pigment epithelium disease in neovascular age-related macular degeneration," Ophthalmology Retina **5**(12), 1204–1213 (2021).

31. T. J. Gin, A. Wu, S. K. H. Chew, *et al.*, "Quantitative analysis of the ellipsoid zone intensity in phenotypic variations of intermediate age-related macular degeneration," Invest Ophthalmol Vis Sci **58**(4), 2079–2086 (2017).

32. B. J. Lujan, A. Roorda, J. A. Croskrey, *et al.*, "Directional optical coherence tomography provides accurate outer nuclear layer and henle fiber layer measurements," Retina **35**(8), 1511–1520 (2015).

33. B. Marsh-Armstrong, K. S. Murrell, D. Valente, *et al.*, "Using directional OCT to analyze photoreceptor visibility over AMD-related drusen," Sci. Rep. **12**(1), 9763 (2022).

34. Q. Zhang, Y. Shi, M. Shen, *et al.*, "Does the outer retinal thickness around geographic atrophy represent another clinical biomarker for predicting growth?" Am. J. Ophthalmol. **244**, 79–87 (2022).

35. A. Gawish, P. Fieguth, S. Marschall, *et al.*, "Undecimated hierarchical active contours for OCT image segmentation," in *2014 IEEE International Conference on Image Processing (ICIP)* (2014), pp. 882–886.

36. S. J. Chiu, J. A. Izatt, R. V. O'Connell, *et al.*, "Validated automatic segmentation of AMD pathology including drusen and geographic atrophy in SD-OCT images," Invest. Ophthalmol. Visual Sci. **53**(1), 53–61 (2012).

37. A. Stankiewicz, T. Marciniak, A. Dąbrowski, *et al.*, "Improving segmentation of 3D retina layers based on graph theory approach for low quality OCT images," Metrology and Measurement Systems **23**(2), 269–280 (2016).

38. S. Mukherjee, T. De Silva, P. Grisso, *et al.*, "Retinal layer segmentation in optical coherence tomography (OCT) using a 3D deep-convolutional regression network for patients with age-related macular degeneration," Biomed Opt Express **13**(6), 3195–3210 (2022).

39. Z. Mishra, A. Ganegoda, J. Selicha, *et al.*, "Automated retinal layer segmentation using graph-based algorithm incorporating deep-learning-derived information," Sci. Rep. **10**(1), 9541 (2020).

40. Y. He, A. Carass, Y. Liu, *et al.*, "Structured layer surface segmentation for retina OCT using fully convolutional regression networks," Med Image Anal **68**, 101856 (2021).

41. I. Z. Matovinovic, S. Loncaric, J. Lo, *et al.*, "Transfer learning with U-Net type model for automatic segmentation of three retinal layers in optical coherence tomography images," in *2019 11th International Symposium on Image and Signal Processing and Analysis (ISPA)* (2019), pp. 49–53.

42. I. A. Viedma, D. Alonso-Caneiro, S. A. Read, *et al.*, "A deep learning multi-capture segmentation modality for retinal OCT imaging," in *2022 International Conference on Digital Image Computing: Techniques and Applications (DICTA)* (2022), pp. 1–8.

43. Y. Zhang, Z. Li, N. Nan, *et al.*, "TranSegNet: hybrid CNN-vision transformers encoder for retina segmentation of optical coherence tomography," Life **13**(4), 976 (2023).

44. A. Shah, L. Zhou, M. D. Abrámoff, *et al.*, "Multiple surface segmentation using convolution neural nets: application to retinal layer segmentation in OCT images," Biomed Opt Express **9**(9), 4509–4526 (2018).

45. J. Schottenhamml, E. M. Moult, S. B. Ploner, *et al.*, "OCT-OCTA segmentation: combining structural and blood flow information to segment Bruch's membrane," Biomed. Opt. Express **12**(1), 84–99 (2021).

46. Y. He, A. Carass, Y. Liu, *et al.*, "Longitudinal deep network for consistent OCT layer segmentation," Biomed. Opt. Express **14**(5), 1874–1893 (2023).

47. H. Zhang, J. Yang, C. Zheng, *et al.*, "Annotation-efficient learning for OCT segmentation," Biomed. Opt. Express **14**(7), 3294–3307 (2023).

48. H. Xie, W. Xu, Y. X. Wang, *et al.*, "Deep learning network with differentiable dynamic programming for retina OCT surface segmentation," Biomed Opt Express **14**(7), 3190–3202 (2023).

49. J. Long, E. Shelhamer, and T. Darrell, "Fully convolutional networks for semantic segmentation," in (*Proceedings of the IEEE Conference on Computer Vision and Pattern Recognition*, 2015), pp. 3431–3440.

50. O. Ronneberger, P. Fischer, T. Brox, *et al.*, eds. (Medical Image Computing and Computer-Assisted Intervention, 2015), pp. 234–241.

51. A. Dosovitskiy, L. Beyer, A. Kolesnikov, *et al.*, "An image is worth 16×16 words: transformers for image recognition at scale," arXiv, arXiv:2010.11929 (2021).

52. J. Chen, Y. Lu, Q. Yu, *et al.*, "TransUNet: transformers make strong encoders for medical image segmentation," arXiv arXiv:2102.04306 (2021).

53. X. Yin, J. R. Chao, and R. K. Wang, "User-guided segmentation for volumetric retinal optical coherence tomography images," J Biomed Opt **19**(8), 086020 (2014).

54. X. Jiang, M. Shen, L. Wang, *et al.*, "Validation of a novel automated algorithm to measure drusen volume and area using swept source optical coherence tomography angiography," Trans. Vis. Sci. Tech. **10**(4), 11 (2021).

55. Z. Chu, L. Wang, X. Zhou, *et al.*, "Automatic geographic atrophy segmentation using optical attenuation in OCT scans with deep learning," Biomed. Opt. Express **13**(3), 1328–1343 (2022).

56. Y. Zhao, J. Zhao, Y. Gu, *et al.*, "Outer retinal layer thickness changes in white matter hyperintensity and Parkinson's Disease," Front. Neurosci. **15**, 741651 (2021).

57. B. J. Kim, D. J. Irwin, D. Song, *et al.*, "Optical coherence tomography identifies outer retina thinning in frontotemporal degeneration," Neurology **89**(15), 1604–1611 (2017).

58. T. F. Eliwa, M. A. Hussein, M. A. Zaki, *et al.*, "Outer retinal layer thickness as good visual predictor in patients with diabetic macular edema," Retina **38**(4), 805–811 (2018).

59. L. Toto, E. Borrelli, R. Mastropasqua, *et al.*, "Association between outer retinal alterations and microvascular changes in intermediate stage age-related macular degeneration: an optical coherence tomography angiography study," Br. J. Ophthalmol. **101**(6), 774–779 (2017).

60. R. F. Spaide, "Outer retinal atrophy after regression of subretinal drusenoid deposits as a newly recognized form of late age-related macular degeneration," Retina **33**(9), 1800–1808 (2013).

61. J. S. Steinberg, M. Saßmannshausen, M. Fleckenstein, *et al.*, "Correlation of Partial Outer Retinal Thickness With Scotopic and Mesopic Fundus-Controlled Perimetry in Patients With Reticular Drusen," Am. J. Ophthalmol. **168**, 52–61 (2016).

62. S. Ooto, M. Hangai, A. Tomidokoro, *et al.*, "Effects of age, sex, and axial length on the three-dimensional profile of normal macular layer structures," Invest Ophthalmol Vis Sci **52**(12), 8769–8779 (2011).

63. S. Arepalli, S. K. Srivastava, M. Hu, *et al.*, "Assessment of inner and outer retinal layer metrics on the Cirrus HD-OCT Platform in normal eyes," PLoS One **13**(10), e0203324 (2018).

64. S. M. Waldstein, W.-D. Vogl, H. Bogunovic, *et al.*, "Characterization of Drusen and Hyperreflective Foci as Biomarkers for Disease Progression in Age-Related Macular Degeneration Using Artificial Intelligence in Optical Coherence Tomography," JAMA Ophthalmol. **138**(7), 740–747 (2020).

65. S. G. Schuman, A. F. Koreishi, S. Farsiu, *et al.*, "Photoreceptor layer thinning over drusen in eyes with age-related macular degeneration imaged in vivo with spectral-domain optical coherence tomography," Ophthalmology **116**(3), 488–496.e2 (2009).

66. D. L. Wang, J. Agee, M. Mazzola, *et al.*, "Outer retinal thickness and fundus autofluorescence in geographic atrophy," Ophthalmol Retina **3**(12), 1035–1044 (2019).

67. T. D. Silva, E. Y. Chew, N. Hotaling, *et al.*, "Deep-learning based multi-modal retinal image registration for the longitudinal analysis of patients with age-related macular degeneration," Biomed. Opt. Express **12**(1), 619–636 (2021).

68. Y. Jia, S. T. Bailey, D. J. Wilson, *et al.*, "Quantitative optical coherence tomography angiography of choroidal neovascularization in age-related macular degeneration," Ophthalmology **121**(7), 1435–1444 (2014).

69. E. M. Moult, N. K. Waheed, E. A. Novais, *et al.*, "Swept source OCT angiography reveals choriocapillaris alterations in eyes with nascent geographic atrophy and drusen-associated atrophy," Retina **36**(Supplement 1), S2–S11 (2016).

70. Q. S. You, J. Wang, Y. Guo, *et al.*, "Detection of reduced retinal vessel density in eyes with geographic atrophy secondary to age-related macular degeneration using projection-resolved optical coherence tomography angiography," Am. J. Ophthalmol. **209**, 206–212 (2020).